Levels of the four lowest two-particle configurations in ^{210}Po studied by in-beam γ-ray and conversion-electron spectroscopy with the ^{209}Bi$(t,2n)$ reaction

L. G. Mann, K. H. Maier,* A. Aprahamian, J. A. Becker, D. J. Decman, E. A. Henry, R. A. Meyer, N. Roy, W. Stöffl, and G. L. Struble
Lawrence Livermore National Laboratory, Livermore, California 94550
(Received 14 March 1988)

We have used the ^{209}Bi$(t,2n)^{210}$Po reaction with standard in-beam γ-ray and conversion-electron spectroscopic techniques to study the two-proton states in ^{210}Po. With the possible exception of the $(f^2_{7/2})_{2^+}$, all states of the proton $h^2_{9/2}$, $h_{9/2}f_{7/2}$, $f^2_{7/2}$, and $h_{9/2}i_{13/2}$ configurations have been identified. The level energies agree within 100 keV, typically, with results from shell-model calculations. Relative intensities of $M1$ and $E2$ γ transitions from the $h_{9/2}f_{7/2}$ and $f^2_{7/2}$ configurations are compared with calculated intensities. Published experimental single-proton transition matrix elements were used for the calculations, which were performed both for pure and for mixed states. The results indicate admixture amplitudes of only a few percent or less into the main components of the wave functions.

I. INTRODUCTION

Nuclei in the immediate vicinity of doubly magic ^{208}Pb provide the best available testing ground for shell-model calculations in the heavy-element region. Therefore, it is particularly important to have complete experimental data in this region. A large amount of experimental information on nuclei near Pb has been obtained through a wide variety of experiments. Nevertheless, there are many gaps in the data. For example, in the two-proton-hole nucleus ^{206}Hg only two of the excited hole states are known. In ^{208}Pb there are no γ-decay data for states with $J>6$, and our knowledge of particle-hole states is very limited. The reason for this situation is that ^{208}Pb is a neutron-rich nucleus and therefore the number of available targets and associated reactions for studying these nuclei is quite limited. In this regard the neutron-rich triton as a projectile offers some unique possibilities. We have previously used the $(t,2n)$ and (t,p) reactions and targets of ^{208}Pb and ^{204}Hg to study ^{209}Bi, ^{210}Pb, ^{205}Tl, and ^{206}Hg with in-beam spectroscopic techniques.[1–4] We have now used these same reactions, and also the (t,α), with ^{209}Bi targets.[5] This paper will present the results from the ^{209}Bi$(t,2n)^{210}$Po reaction; the results of the concurrent studies of ^{211}Bi and ^{208}Pb from the other reactions will be published separately.

In ^{210}Po, which has two protons outside the ^{208}Pb core, the lowest-lying configurations are the $\pi h^2_{9/2}$, $\pi h_{9/2}f_{7/2}$, $\pi h_{9/2}i_{13/2}$, and $\pi f^2_{7/2}$, resulting in a total of 27 energy levels. The only other levels expected in this energy region are the collective 3^- and the $\nu g_{9/2}p^{-1}_{1/2}$ core states. Most of the existing information[6] on ^{210}Po has been obtained from charged-particle spectroscopic studies[7] associated with proton transfer to ^{209}Bi targets, in-beam γ-ray spectroscopy[8,9] with the ^{208}Pb$(\alpha,2n)$ reaction, and γ-ray and electron spectroscopy[10] for levels populated by β decay of the $J^\pi=5^+$ ground state of ^{210}At. These studies have produced no information at all about the levels of the $f^2_{7/2}$ configuration, and for the $h_{9/2}f_{7/2}$ and $h_{9/2}i_{13/2}$ configurations with $J\leq 3$ the data are particularly inadequate or nonexistent. In addition, much more information is needed about γ-decay properties, which are a sensitive probe of the wave functions.

The ^{209}Bi$(t,2n)$ reaction populates (with useful intensities) states having a wide range of spins, including levels up to $\sim$2 MeV above the yrast line. Therefore we used this reaction with γ-ray and electron spectroscopy to study ^{210}Po. The goals were to locate the missing states of the two-proton configurations, to solidify other spin-parity assignments, and to obtain γ-ray branching intensities for use in testing shell-model calculations.

II. EXPERIMENTS

The experimental measurements were carried out at our in-beam nuclear spectroscopy facilities at the Los Alamos National Laboratory (LANL) tandem Van de Graaff accelerator. We measured γ-ray excitation functions, γ-γ coincidences, and γ-ray and electron energy spectra for the reactions ^{209}Bi$+t$. Triton energies were 11.5, 12, 13, 15, and 17 MeV in the excitation-function runs, 13 and 17 MeV for the γ-γ coincidence experiments, and 13 MeV for the electron measurements. We chose a low bombarding energy for most of the experiments in order to enhance the population of lower-spin states above the yrast line. All the experiments were performed with a pulsed triton beam ($\sim$1–3 μs between pulses, typically) in order to obtain decay information for the numerous isomeric states. The targets were metallic Bi, 10-mg/cm^2 thick for the excitation functions, 200 mg/cm^2 for the coincidence experiments, and 500 μg/cm^2 on 20-μg/cm^2 carbon backing for the conversion-electron measurements.

The two γ-ray detectors used in the coincidence experiments were high-purity Ge of the coaxial gamma-X type with efficiencies of 21% for ^{60}Co γ rays in the standard comparison with NaI. One of them was operated with a

bismuth germanate (BGO) anti-Compton shield. In this arrangement the peak/total count ratio was 27% and the energy resolution was 2.2 keV full width at half maximum (FWHM) for ^{60}Co γ rays. The two detectors were on opposite sides of the beam line, at 80° from the forward direction and as close as possible to the target during the coincidence runs. The distance from the target to the centers of the detectors was about 11 cm for the BGO-shielded detector and 5 cm for the unshielded detector. Copper absorbers 2-mm thick were placed in front of both detectors. The BGO-shielded detector was also used in the excitation-function experiments for γ-ray energies and absolute intensities. Standard radioactive sources of ^{133}Ba, ^{60}Co, and ^{152}Eu placed at the in-beam target position provided calibration data for energy and absolute efficiency.

All the transition intensities are expressed in millibarns, based on the integrated beam current, target thickness, and detector efficiencies (including solid angle). We estimate a total error of ±20% in the conversion to millibarns. The largest contribution to this error comes from the uncertainty in the orientation of the target plane, which was between 45° and 60° away from the beam line during the excitation-function runs. Therefore, the 10-mg/cm^2 target had an effective thickness of 12.8±1.4 mg/cm^2.

Figure 1 shows the excitation functions for several γ-ray ground-state transitions that are representative of the total strengths of the competing reactions. At $E_t = 13$ MeV, which is about 10 MeV above the $(t,2n)$ threshold and 2 MeV above the Coulomb barrier, no competing reaction has more than a few percent of the $(t,2n)$ strength. The 2290.1- and 2393.8-keV γ rays from low-spin states

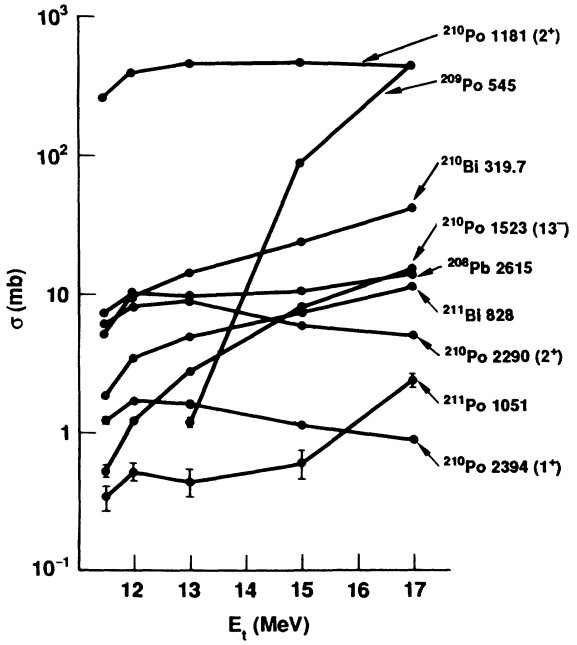

FIG. 1. Gamma-ray excitation functions for the reaction ^{209}Bi+t. Labels give the product nuclide and the γ-ray energy in keV, and for transitions in ^{210}Po, the spin and parity of the γ-emitting state.

and the 1522.8-keV γ ray from the 13$^-$ state in ^{210}Po illustrate how the energy dependence of the $(t,2n)$ cross section changes for different final-state spins. These experiments were most effective for studying the states of lower spins, by using a low triton energy.

The electron spectrometer[11] consists of a superconducting solenoidal magnet transporter with an energy dispersive Si(Li) detector. The detector was 5.5-mm thick, which gives full detection efficiency for electron energies up to about 2.0 MeV. Electron spectra were obtained in four different energy ranges by making multiple sweeps of the magnetic field in linear stepwise fashion over the specified range of energies. For each sweep range the efficiency curve was determined by sweeping in identical fashion with a ^{152}Eu calibration source at the in-beam target position. It would have been preferable for calibration purposes if the entire energy range from < 100 keV up to about 2700 keV could have been covered in only one or two long sweeps, but this was impractical because of the large differences in count rates for different energy regions.

Figure 2 shows the electron relative efficiency curves obtained from the ^{152}Eu data for each of the four sweep ranges. Each curve was normalized independently to the ^{210}Po electron and γ-ray data by using one or more lines of known multipolarity from the in-beam data. It was necessary to extend the calibration of the highest sweep to higher energies than the maximum of 1400 keV available from ^{152}Eu. For this extension we used the 2615-keV $E3$ transition in ^{208}Pb produced by the (t,α) reaction in the ^{209}Bi target, and also an earlier calibration obtained from the ^{144}Sm$(t,2n)^{145}$Eu reaction[12] which establishes the shape of the curve between 1000 and 2000 keV. In the region between 2000 keV and the ^{208}Pb calibration point there are two γ-ray transitions to the 0$^+$ ground state from levels at 2290.1 and 2393.8 keV in ^{210}Po. Groleau *et al.*[7] have assigned values of $J^\pi = 2^+$ and 1^+, respectively, to these levels, although the latter level presented a severe resolution problem in their experiments. We made the assumption of either pure $M1$ or $E2$ multipolarity for each of these γ rays and show the re-

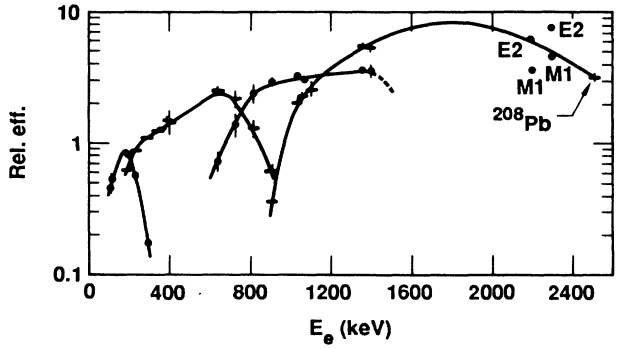

FIG. 2. Relative electron detection efficiencies for the four energy ranges swept by the electron spectrometer. The four points labeled $M1$ or $E2$ are from the 2290.2- and 2398.8-keV transitions in ^{210}Po, under the assumptions of $M1$ or $E2$ multipolarity. All the unlabeled points are from transitions of known multipolarity in ^{152}Eu decay.

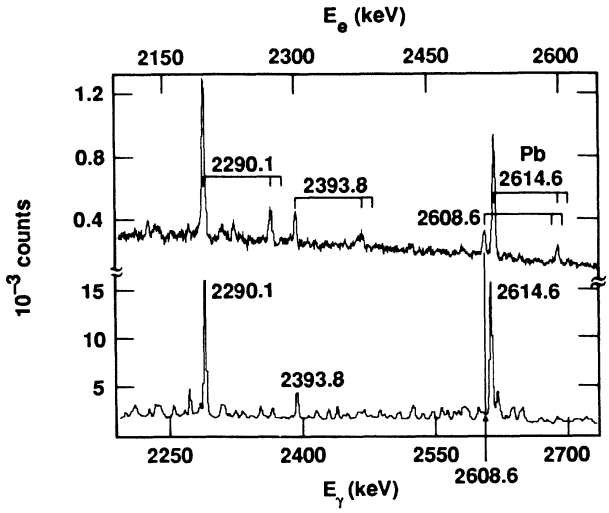

FIG. 3. A high-energy portion of the electron (top) and γ-ray (bottom) spectra obtained from ^{209}Bi$+t$ at $E_t=13$ MeV. Peaks are labeled by the γ-ray energy in keV and by the positions of the K, L, and M conversion-electron peaks. The horizontal scales of the two spectra have been adjusted so that associated γ-ray and K-electron peaks from transitions in Po line up vertically.

sulting calibration points in Fig. 2. Clearly, $E2$ for the 2290.1-keV and $M1$ for the 2393.8-keV γ rays are the only multipolarities that are compatible with a smooth calibration curve, strongly supporting the spin-parity assignments of Groleau *et al.* and giving added confidence in our calibration curve. Figure 3 shows the electron and γ-ray spectra in this region, including the 2615-keV transition in ^{208}Pb.

In each experiment two-parameter data arrays consisting of 4096 or 8192 channels of energy and 256 or 128 channels of time information were accumulated in the megaword memory of the LANL computer-based data system.[13] In addition, for the coincidence experiments four-parameter data consisting of the energies E_1 and E_2 from the two detectors and their times t_1-t_0 and t_2-t_0 with respect to the beam pulses were accumulated event-by-event on magnetic tape. Coincident γ-ray spectra were generated off line by sorting the event data with appropriate energy and prompt or delayed time gates. We used the FITEK (Ref. 14) code to analyze the spectra for energies and intensities.

The electron spectra are complicated because of multiple peaks generated by conversion in the many atomic subshells. The flexibility of FITEK enabled us to relate the energies and, if the multipolarity was known, intensities of the L and M subshell peaks to the associated K peak. This greatly enhanced our ability to determine electron intensities in complex regions of the spectra.

III. RESULTS

Our experimental results are summarized in Table I and the level scheme of Fig. 4. In these summary presentations we use parentheses to denote the most likely choices for spins and parities that are not uniquely determined. Alternative possibilities are discussed in the text. The γ-ray energies in Table I are weighted averages of the values obtained from the five excitation-function runs, at bombarding energies of 11.5, 12, 13, 15, and 17 MeV. Not all the γ rays could be measured at all five bombarding energies. The level energies in Table I were obtained by a least-squares fit to all the γ-ray combinations involving the level. The decay scheme of Fig. 4 is supported by energy fits (Ritz principle), γ-γ coincidence data, and γ-ray multipolarities obtained from the conversion-coefficient measurements. There is good agreement between our conversion coefficients in Table I and those measured by Jardine *et al.*,[10] except for the K lines of the 724.9- and 615.3-keV γ rays, where we disagree by 3–4 standard deviations. Figures 5–7 show some of the γ-γ coincidence spectra that support new aspects of the decay scheme.

Previously published work, summarized in Ref. 6, has characterized the known levels below 3219.0 keV in terms of the two extra-core protons and the core 3^- and $\nu g_{9/2}p_{1/2}^{-1}$ states. All the levels of the $\pi h_{9/2}^2$ ground-state configuration have been well studied. We have observed at least four new levels associated with the other two-proton configurations in this region and have determined definite or more restrictive assignments for several other levels whose spins or parities were uncertain. Some of the levels above 3219.0 keV of excitation have also been characterized in the earlier studies. We see several new levels in the region between 3220 and 5000 keV and we make definite or more restrictive spin-parity assignments than was previously possible for several other levels. In the following subsections we will discuss the evidence for the new states and new assignments.

A. The $\pi h_{9/2}f_{7/2}$ configuration

The β-decay experiments[10] and the $(\alpha,2n)$ in-beam studies[8] have identified all the higher-spin levels, from 4^+ to 8^+, of this configuration. There was no evidence for the other three states, with $J^\pi=1^+$, 2^+, and 3^+, in the $(\alpha,2n)$ experiments, and only a very tentative proposal for the 2^+ state could be made from the decay data, based on a 2290.0-keV ground-state gamma transition and a weak 92.0-keV transition from the 4^+ level at 2382.6 keV. Groleau *et al.*[7] used l-transfer data and spectroscopic factors to associate all the states of the $\pi h_{9/2}f_{7/2}$ configuration with levels they observed in the (^{4}He,t) and (^{3}He,d) reactions. They assigned values of $J^\pi=1^+$, 2^+, and 3^+, respectively, to levels at 2391, 2290, and 2412 keV.

We see γ rays of 2290.1 and 2393.8 keV whose excitation functions are typical of low-spin states (Fig. 1). These γ rays do not appear in the coincidence data, indicating that they populate the ground state directly from levels at 2290.1 and 2393.8 keV. Weak γ-ray branches of 1108.6 and 1212.2 keV, respectively, from these levels to the 2_1^+ level appear in coincidence with the 1181.4-keV γ ray (Fig. 6) and exhibit excitation functions typical of low-spin levels. The conversion coefficients, discussed in Sec. II, require $J^\pi=2^+$ and 1^+, respectively, for the 2290.1- and 2393.8-keV levels.

TABLE I. Results of in-beam γ-ray and conversion-electron measurements for ^{210}Po produced by the ^{209}Bi(t,2n) reaction at $E_t = 13.0$ MeV.

	Level[a]			Depopulating γ ray[a]						Final state[a]	
		J^π			$I(\Delta I)$[b]	$10^3\times$conv. coef.[c]			γ-ray		
	$E(\Delta E)$	(t,2n)	Ref. 6	$E(\Delta E)$	(mb)	K	L	Mult.[d]	branch (%)	E_f	J_f^π
1	0	0^+	0^+								
2	1181.40(2)	2^+	2^+	1181.39(1)	459(2)	4.19	0.76(7)	$E2$	100	0	0^+
3	1426.70(1)	4^+	4^+	245.31(1)	308(1)	106	99	$E2$	100	1181.40	2^+
4	1473.34(2)	6^+	6^+	46.6				$E2$	100	1426.70	4^+
5	1556.96(3)	8^+	8^+	83.69	143(30)[e]			$E2$	100	1473.34	6^+
6	2187.96(3)	8^+	8^+	630.97(1)	56.4(2)	50.2	8.8	0.79(3)$M1$[f]	100	1556.96	8^+
7	2290.10(4)	2^+	(2^+)	2290.22(5)	9.0(2)	1.32	0.27(5)	$E2$	90	0	0^+
				1108.55(7)	1.01(10)	11.5(18)		0.73(20)$M1$	10	1181.40	2^+
8	2326.00(2)	6^+	6^+	899.23(14)	0.58(9)				1.8	1426.70	4^+
				852.66(1)	29.9(3)	22(2)		0.74(10)$M1$	95	1473.34	6^+
				769.20(6)	1.10(8)				3.5	1556.96	8^+
9	2382.55(2)	4^+	4^+	1201.46(13)	0.96(13)	5.4(10)		$E2$	6	1181.40	2^+
				955.84(1)	14.1(2)	17(2)	3.3(4)	0.82(11)$M1$	89	1426.70	4^+
				909.00(8)	0.83(6)				5	1473.34	6^+
10	2386.78(2)	3^-	3^-	1205.38(2)	19.6(3)	1.6(2)	0.22(3)	$E1$	90	1181.40	2^+
				960.01(5)	2.22(12)	2.4(4)		$E1$	10	1426.70	4^+
11	2393.76(6)	1^+	(1^+)	2393.79(7)	1.63(8)	1.97		$M1$	73	0	0^+
				1212.18(16)	0.6(1)				27	1181.40	2^+
12	2403.27(2)	5^+	5^+	976.55(2)	7.92(14)	14(2)	3.7(6)	0.73(13)$M1$	48.5	1426.70	4^+
				929.93(2)	7.89(16)	16.0(12)	3.2(4)	0.66(7)$M1$	48.2	1473.34	6^+
				77.27	3.0(8)[g]				3.2	2326.00	6^+
				20.72	1.8(11)[g]				0.07	2382.55	4^+
13	2413.77(3)	3^+	(3^+)	1232.36(3)	4.50(16)	6.6(5)	1.5(2)	0.43(7)$M1$	80	1181.40	2^+
				987.12(10)	0.71(10)	20(3)		$M1$	13	1426.70	4^+
				123.77(10)	0.38(6)		1700(400)	$M1/E2$	7	2290.10	2^+
14	2438.35(3)	7^+	7^+	965.01(3)	4.29(1)	13.1(5)		0.50(11)$M1$	27	1473.34	6^+
				881.39(2)	6.45(14)	21(2)		0.76(11)$M1$	40	1556.96	8^+
				250.35(3)	4.9(3)	920(200)		($M1$)	30	2187.96	8^+
				112.29(10)	0.42(7)				3	2326.00	6^+
15	2608.56(7)	0^+		2608.56(10)[h]	<0.5	>7		$E0$	0.061(15)[i]	0	0^+
				1427.2(1)[j]	0.47(23)[k]	3.5(17)		$E2$		1181.40	2^+
				214.80(8)[l]	<0.2[j]					2393.76	1^+
16	2845.96(7)	$(3)^-$		1664.57(7)	1.76(15)	1.6(2)		0.94(2)$E1$	73	1181.40	2^+
				459.0(3)	0.66(30)	124(60)	26(12)	$M1$	27	2386.78	3^-
17	2849.16(3)	11^-	11^-	1292.20(1)	41.0(3)	7.68	1.83(10)	$E3$	95	1556.96	8^+
				661.17(3)[m]	2.0(1)[m]	27(3)	13(1)	$E3$	5	2187.96	8^+
18	2910.05(2)	5^-	5^-	1483.39(2)	12.3(2)	1.1(1)		$E1$	62	1426.70	4^+
				1436.70(2)	7.5(2)	1.4(1)		$E1$	37	1473.34	6^+
				527.4(2)	0.19(4)				1	2382.55	4^+
19	2999.48(3)	$(9)^-$	(9^-)	1442.60(3)	3.34(16)	1.7(2)		0.97(1)$E1$	24	1556.96	8^+
				811.51(1)	10.3(2)	3.4(5)		$E1$	76	2181.96	8^+
20	3016.47(3)	7^-	(7^-)	1543.14(2)	4.58(11)	0.93(10)		$E1$	77	1473.34	6^+
				690.6(2)[k]	1.6(3)[m]				26	2326.00	6^+
				578.01(5)	0.90(8)	17(4)		0.94(2)$E1$	12	2438.35	7^+
21	3023.73(4)	$(2)^-$		636.95(5)	1.72(9)	58(7)	8.8(13)	$M1$	77	2386.78	3^-
				609.94(10)	0.51(10)				23	2413.77	3^+

TABLE I. (*Continued*).

	Level[a]			Depopulating γ ray[a]						Final state[a]	
	$E(\Delta E)$	J^π $(t,2n)$	Ref. 6	$E(\Delta E)$	$I(\Delta I)$[b] (mb)	$10^3\times$conv. coef.[c] K	L	Mult.[d]	γ-ray branch (%)	E_f	J_f^π
22	3026.42(2)	5^-	5^-	1599.70(2)	6.4(2)	0.90(10)		$E1$	82	1426.70	4^+
				1553.0(5)	$\lesssim 0.05$				1	1473.34	6^+
				639.56(16)	0.5(2)	14(7)		($E2$)	6	2386.78	3^-
				622.83(23)	0.25(8)				3	2403.27	5^+
				116.47(3)	0.63(8)		1300(200)	$M1$	8	2910.05	5^-
23	3075.13(3)	$(4)^-$	(4^-)	1648.45(3)	2.64(9)	0.92(10)		$E1$	56	1426.70	4^+
				692.4(2)[k]	0.4(2)[m]				9	2382.55	4^+
				688.2(1)[k]	1.4(2)[k]				30	2386.78	3^-
				661.1(3)[k]	0.23(7)[m]				5	2413.77	3^+
24	3094.52(14)	4^+		1913.10(21)	0.28(5)	2.2(9)		$E2$	8	1181.40	2^+
				1667.9(5)[k]	0.24(10)[k]				7	1426.70	4^+
				768.9(5)[k]	0.31(13)[k]				9	2326.00	6^+
				691.2(2)[k]	2.8(4)[m]	38(8)	6.0(12)	0.69(20)$M1$	76	2403.27	5^+
25	3111.64(2)	4^-	$(4)^-$	1684.6(4)[k]	0.48(15)[k]	<1.5		$E1$	9	1426.70	4^+
				728.4(4)[k]	0.3(1)	20(10)			4	2382.55	4^+
				724.86(2)	3.6(4)	26(4)	4.7(7)	0.49(13)$M1$	67	2386.78	3^-
				201.60(3)	1.05(15)[n]	1300(250)	300(60)	$M1$	20	2910.05	5^-
26	3125.13(3)	$(6)^-$	(6^-)	799.19(4)	1.27(10)	≤ 3	<1.4	$E1$	37	2326.00	6^+
				721.84(3)	2.3(2)	5.3(13)		$E1$	63	2403.27	5^+
27	3138.00(4)	$(8)^-$	(8^-)	1581.09(4)	1.45(9)	1.8(2)		0.94(2)$E1$	35	1556.96	8^+
				949.97(4)	1.45(11)	3.6(8)	<0.9	0.98(1)$E1$	35	2187.96	8^+
				699.51(25)[k]	1.2(2)[k]	6.1(21)		$E1$	30	2438.35	7^+
28	3182.77(3)	10^-	(10^-)	1625.91(6)	0.85(8)	10.5(14)		0.84(20)$M2$	11	1556.96	8^+
				333.61(2)	5.70(12)	270(30)	54(7)	$M1$	74	2849.16	11^-
				183.31(3)	1.13(14)	1700(430)	400(70)	$M1$	15	2999.48	$(9)^-$
29	3218.98(4)	$(6)^+$		1745.98(29)	0.7(3)	2.4(11)		0.1(5)$M1$	16	1473.34	6^+
				1030.6(5)[k]	0.27(11)[k]				6	2187.96	8^+
				780.62(3)	3.49(9)	28(3)		0.74(12)$M1$	78	2438.35	7^+
30	3428.58(2)	5^-	$(5)^-$	1955.14(6)	0.90(6)	0.59(10)		$E1$	19	1473.34	6^+
				1046.3(3)[k]	0.32(4)[k]				7	2382.55	4^+
				1041.7(3)[k]	0.7(2)[k]		2.3(12)	($E2$)	15	2386.78	3^-
				518.5	0.4(2)[k]				8	2910.05	5^-
				402.15(2)	1.99(5)	190(20)	34(4)	$M1$	42	3026.42	5^-
				316.99(9)	0.41(3)				9	3111.64	$(4)^-$
31	3525.34(3)	6^-	$(6)^-$	2052.1(3)	0.26(6)	<1.2		($E1$)	6	1473.34	6^+
				1122.0(2)[k]	1.3(3)[k]	5.6(25)		0.87(9)$E1$[o]	29	2403.27	5^+
				1087.02(6)	0.91(10)	4.7(10)		0.92(3)$E1$[o]	20	2438.35	7^+
				615.26(4)	1.52(9)	37(5)		0.45(9)$M1$	34	2910.05	5^-
				499.06(7)	0.48(3)	140(30)		$M1$	11	3026.42	5^-
32	3685.39(4)	7^-		2211.81(22)	0.73(10)	0.42(14)		$E1$	19	1473.34	6^+
				2128.08(15)	0.70(6)	$\lesssim 0.5$		$E1$	18	1556.96	8^+
				1497.41(5)	1.62(8)	1.04(14)		$E1$	43	2187.96	8^+
				1359.55(7)	0.75(8)				20	2326.00	6^+
33	3699.59(6)	$(5)^-$		2272.86(7)	1.58(9)	0.54(10)		$E1$	51	1426.70	4^+
				2226.61(14)	0.50(8)	1.9(6)		0.73(12)$E1$	16	1473.34	6^+
				1409.4(2)[j]	<0.3	>5		$M2/E3$?	<10	2290.10	2^+
				1373.58(22)	0.4(1)				13	2326.00	6^+
				1312.39(20)	0.30(6)	5.1(17)		$E2$	10	2386.78	3^-

TABLE I. (*Continued*).

	Level[a]			Depopulating γ ray[a]						Final state[a]	
		J^π			$I(\Delta I)$[b]	$10^3\times$conv. coef.[c]			γ-ray		
	$E(\Delta E)$	$(t,2n)$	Ref. 6	$E(\Delta E)$	(mb)	K	L	Mult.[d]	branch (%)	E_f	J_f^π
34	3710.99(9)	(5^-)		2284.42(11)	0.64(10)				39	1426.70	4^+
				2238.17(23)	0.61(8)	$\lesssim 1$		$(E1)$	38	1473.34	6^+
				1307.26(15)	0.38(8)				23	2403.27	5^+
35	3727.28(6)	$(6)^-$	$(6)^-$	2254.28(12)	0.7(1)	0.7(2)		$E1$	24	1473.34	6^+
				1289.29(16)	0.88(12)				31	2438.35	7^+
				817.23(10)	1.0(1)	24(3)	5.6(10)	0.78(15)$M1$	35	2910.05	5^-
				298.38(10)	0.19(3)				7	3428.58	5^-
				201.6	0.09[p]				3	3525.34	6^-
36	3779.91(6)	$(4,5)^-$		2353.02(9)	0.78(7)	$\lesssim 0.6$		$E1$	48	1426.70	4^+
				870.01(8)	0.83(11)	17(3)		0.5(6)$M1$	52	2910.05	5^-
37	3780.19(5)	$(7)^-$		1592.25(3)	2.8(1)	1.51(14)		0.96(2)$E1$	90	2187.96	8^+
				1453.7(2)	0.3(1)	<1.5		$>0.97E1$	10	2326.00	6^+
38	4025.78(5)	(7–9)		2469.11(14)	0.61(8)	<0.7		$>0.95E1$	21	1556.96	8^+
								0.75(4)$E1$	79	2187.96	8^+
				1837.79(3)	2.31(9)	2.8(3)			79		
								0.47(16)$M1$			
39	4145.41(6)	$(10)^-$		1146.47(20)	0.23(9)	27(12)		$(M1)$	10	2999.48	$(9)^-$
				962.61(7)	2.01(13)	16(2)	3.8(10)	$M1$	90	3182.77	10^-
40	4324.11(3)	11^-	11^-	2767.12(35)	0.29(4)				3	1556.96	8^+
				1474.94(1)	8.14(2)	6.6(7)	1.0(1)	$M1$	90	2849.16	11^-
				178.81(1)[m]	0.63(16)[m]				7	4145.41	$(10)^-$
41	4371.94(3)	13^-	13^-	1522.79(2)	2.70(10)	2.75		$E2$	99	2849.16	11^-
				47.8	4.6(3)[q]				1	4324.11	11^-
42	4502.80(7)	(12^-)		1653.43(15)	0.57(7)	4.2(7)		$(M1)$	51	2849.16	11^-
				357.13(10)	0.12(4)				11	4145.41	$(10)^-$
				178.8(2)[m]	0.42(15)[m]				38	4324.11	11^-
43	4777.28(8)	14^-	14^-	405.5(5)	9.9(10)[r]				93	4371.94	13^-
				274.20(7)	0.74(10)[r]				7	4502.80	$(12)^-$
44	4971.29(14)	$(11^-,12^-)$		825.44(27)	0.90(24)[r]				6	4145.41	$(10)^-$
				599.51(16)[k]	13(4)[k,r]				94	4371.94	13^-
45	5057.61(4)	16^+	16^+	685.69(2)	12.2(4)[r]				92	4371.94	13^-
				279.89(10)	1.1(1)[r]				8	4777.28	14^-

[a]Energies are in keV. Statistical errors in the least significant digits are given in parentheses. Energies quoted with no error were not measured directly in this work.

[b]The intensity errors are statistical only. The accuracy of the calibration for millibarns is estimated to be ±20%.

[c]The conversion coefficients shown without errors were assumed to be known and were used for efficiency calibration of the electron spectrometer.

[d]For mixed transitions we give the fractional intensity of the lowest-order multipole.

[e]Total transition intensity, obtained from L-electron intensities by using the the indicated multipolarity.

[f]Determined from K/L_{12} and L_{12}/L_3 conversion ratios.

[g]Total transition intensity, obtained from γ-ray coincidence data. Gamma intensities derived by assuming $M1$ multipolarity.

[h]Based on K-conversion electrons. $I_K(e^-)=0.0038(6)$ mb.

[i]X_{211} value for $B(E0)/B(E2)$, as discussed in text.

[j]From K-conversion electrons.

[k]From γ-γ coincidence data.

[l]Speculative placement, based on energy only. Detected in the 15- and 17-MeV runs only.

[m]Unresolved multiplet. Intensity splitting determined by γ-γ coincidence data.

[n]Observed intensity reduced by 8% for contribution from decay of the 3727.3-keV level (Ref. 10).

[o]The conversion coefficient would also agree with pure $E2$.

[p]Based on $I_{201.6}/I_{817.2}$ from Ref. 10.

[q]Total transition intensity, determined from γ-ray branchings in delayed spectra.

[r]Measured at $E_t=17$ MeV.

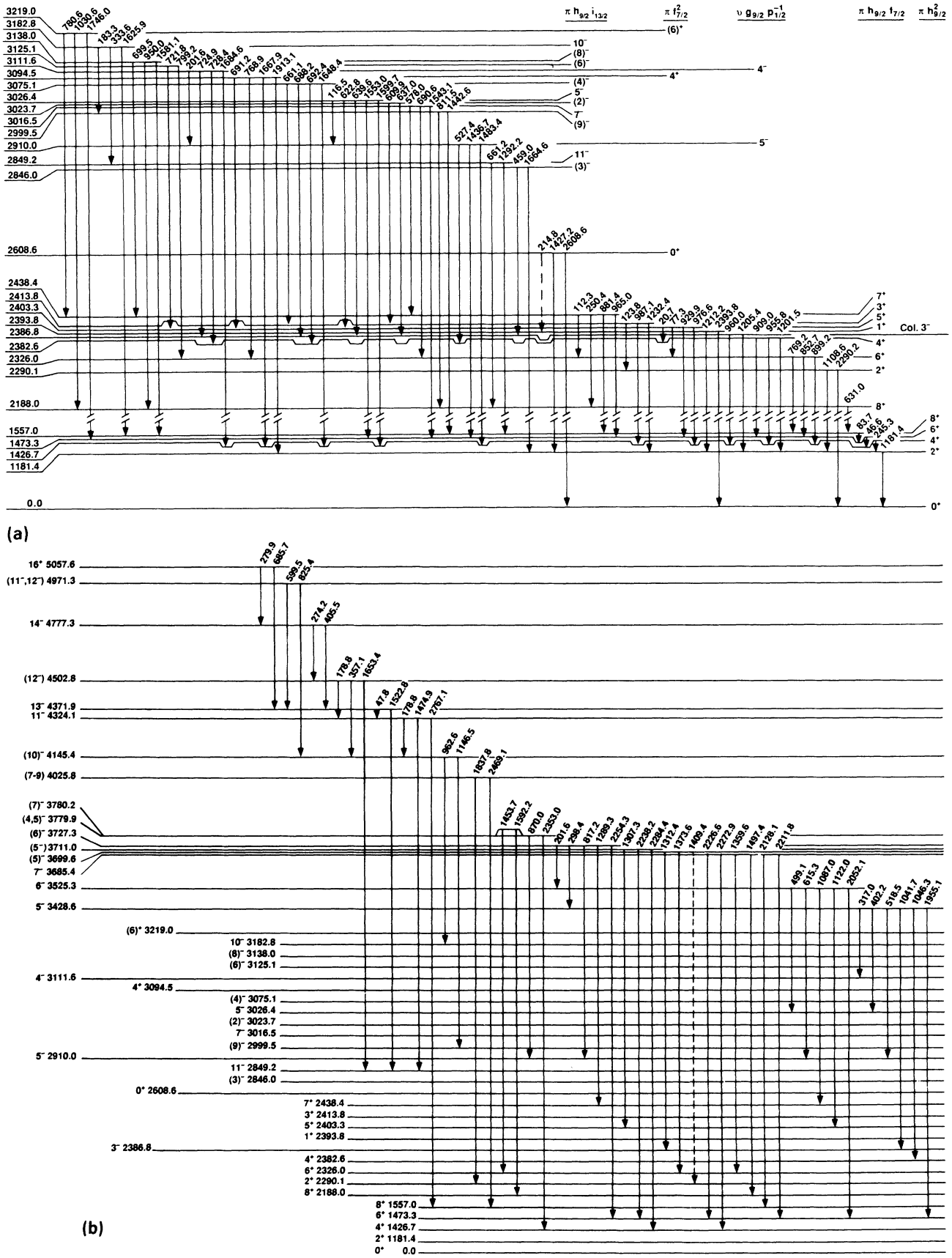

FIG. 4. Decay scheme of levels in ^{210}Po populated by the ^{209}Bi(t,2n) reaction. Energies are in keV. The vertical scale changes by a factor of 8 at 2188.0 keV in (a).

Figures 5 and 6 show that the 1232.4- and 987.1-keV γ rays depopulate the 2413.8-keV level in coincidence with the 1181.4-keV $2_1^+ \rightarrow 0_1^+$ transition. The 987.1-keV γ ray appears clearly in coincidence with the 245.3-keV $4_1^+ \rightarrow 2_1^+$ transition (not shown). The energies of the three depopulating γ rays, to the 2_1^+, 4_1^+, and 2_2^+ levels, fit well in the level scheme, and the excitation functions indicate a low spin. The conversion coefficients, indicating an $M1$ component in each of the depopulating γ rays, require $J^\pi = 3^+$ for the 2413.8-keV level.

Our results for the other five states of the $\pi h_{9/2} f_{7/2}$ configuration, with $J^\pi = 4^+$ to 8^+, agree well with the

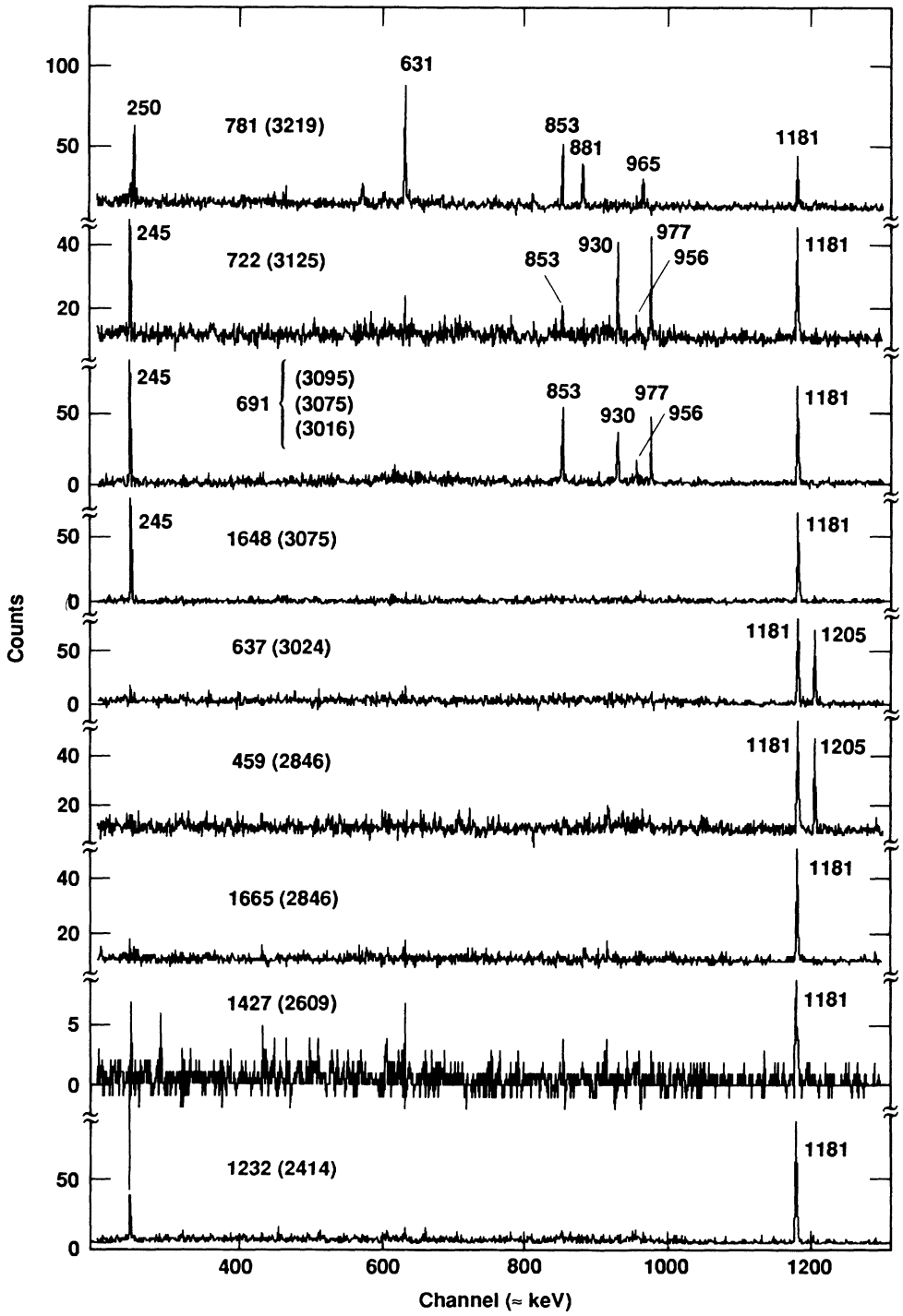

FIG. 5. Spectra from γ-γ coincidences at $E_l = 13$ MeV, for selected γ-ray gates. Peak energies are labeled in keV, and each spectrum is labeled by the energies of the gated γ-ray and (in parentheses) its parent level.

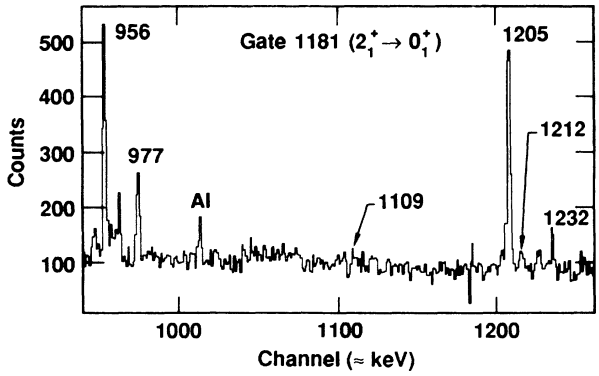

FIG. 6. A portion of the γ-ray spectrum in coincidence with the 1181.4-keV γ ray for $E_t = 13$ MeV.

published reaction and decay data. However, our coincidence data require two low-energy intramultiplet transitions, of 20.7 and 77.3 keV, from the 5^+ level at 2403.3 keV to the 4_2^+ and 6_2^+ levels, respectively. These transitions could not be detected directly because of their low energies and high conversion coefficients. There was previous evidence of the 77.3-keV transition in conversion-electron data of Hoff and Hollander.[15] Our evidence for these two transitions comes from the spectrum in coincidence with the 721.8-keV γ ray which populates the 2403.3-keV level (Fig. 5). The 955.8- and 852.7-keV γ rays appear in this spectrum, and their intensities relative to the 929.9- and 976.6-keV γ rays which depopulate the 2403.3-keV level give respectively the 20.7- and 77.3-keV intensities.

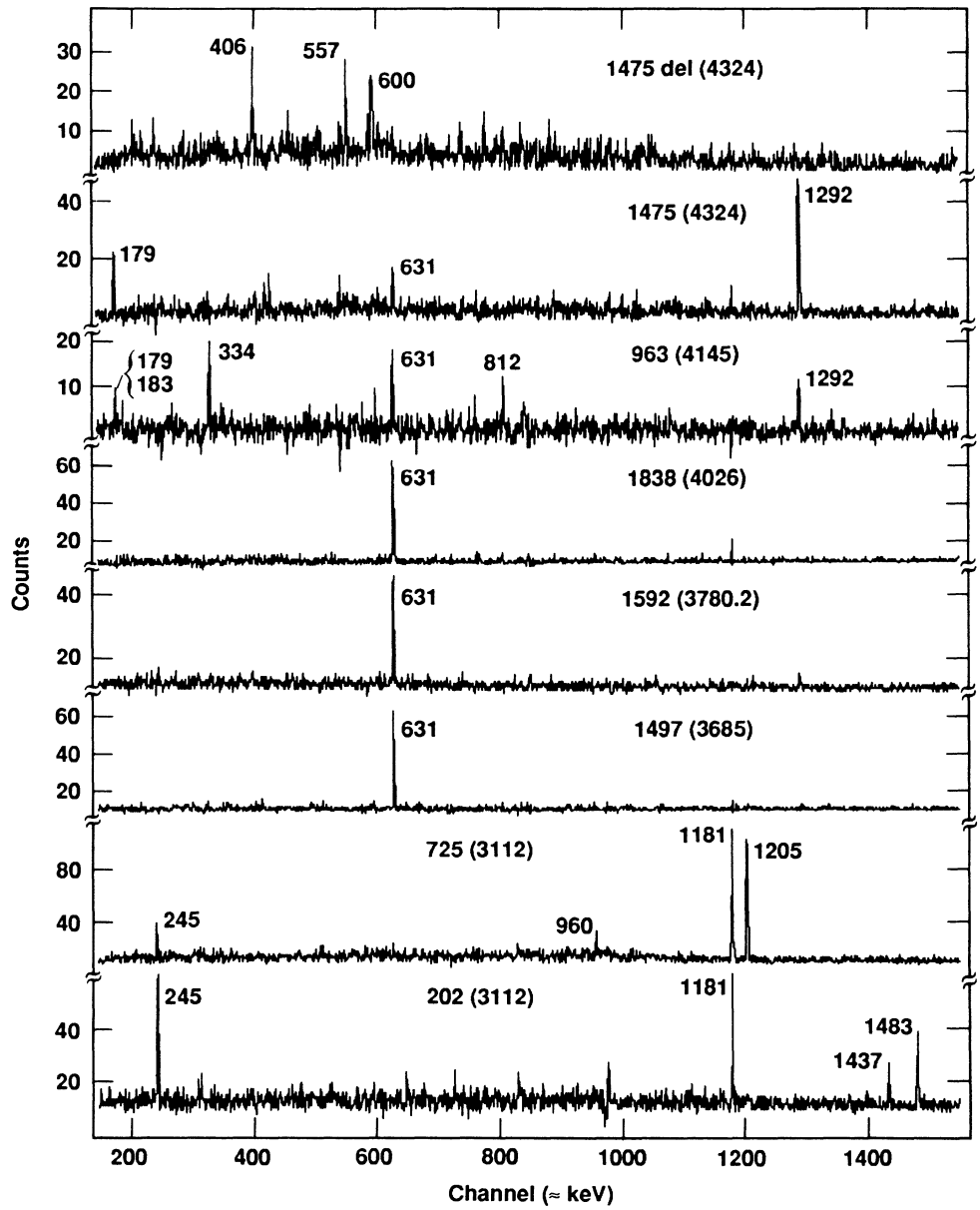

FIG. 7. Same as Fig. 5, except $E_t = 17$ MeV for the 963- and 1475-keV gates (top 3 spectra).

B. The $\pi f_{7/2}^2$ configuration

None of the states of the $\pi f_{7/2}^2$ configuration have previously been identified experimentally. We find three new levels, at 2608.6, 3094.5, and 3219.0 keV, that are good candidates for the 0^+, 4^+, and 6^+ members of this quartet. The evidence for the 2608.6-keV level consists of the K- and L-conversion electron peaks shown in Fig. 3 and a weak 1427.2-keV γ-ray branch to the 2_2^+ level. Table II shows the measured electron energies in the 2600-keV region. Although the L-electron peak of the 2608.6-keV transition is very weak, its energy is consistent with the K-peak energy only for conversion in Po. It is clear in Fig. 3 that any γ ray associated with the 2608.6-keV transition would have a higher multipolarity than the 2614.6-keV $E3$ transition in ^{208}Pb. Our upper limit for the γ-ray intensity gives $\alpha_K > 0.007$, which would require a multipolarity greater than $M3$ or $E4$ and hence a lifetime several orders of magnitude longer than we observe. Therefore, this must be an $E0$ transition from a level at 2608.6 keV.

A weak 1427.2-keV γ-ray branch from this level to the 1181.4-keV level provides additional support for the assignment. This γ ray is difficult to detect because of interference from a much stronger 1426.7-keV peak caused by summing of the $4_1^+ \rightarrow 2_1^+$ and $2_1^+ \rightarrow 0_1^+$ γ transitions in the γ-ray detector. However, the energy and intensity of the K-conversion electrons were obtained from the electron spectrometer, which does not have the summing problem. Also, Fig. 5 shows that the 1181.4-keV $2_1^+ \rightarrow 0_1^+$ γ ray appears in coincidence with the 1427.1-keV gating γ ray. This spectrum provided a rough measurement of the γ intensity and, hence, a K-conversion coefficient, which indicates $E2$ multipolarity. From the ratio of the $E0$ and $E2$ K-conversion electron intensities we derived[16] the value of

$$X_{211} = \frac{B(E0;0_2^+ \rightarrow 0_1^+)}{B(E2;0_2^+ \rightarrow 2_1^+)} = 0.061 \pm 0.015 \ .$$

We see four γ rays that depopulate the level at 3094.5 keV. The strongest γ transition from this level has an energy of 691.2 keV and populates the 5_1^+ state. This γ ray presents a serious measurement problem, both because of strong interference caused by fast-neutron excitation of the 691.3-keV state in the Ge detectors and because there is a triplet of γ rays in ^{210}Po at this energy. Therefore, all the energy and intensity data for the 691.2-keV γ ray were obtained from the strong coincidences with the 929.9- and 976.6-keV γ rays that depopulate the 5_1^+ state. In Fig. 5, a comparison of the spectra in coincidence with the 691- and 721.8-keV gates shows enhanced intensities of the 852.7- and 955.8-keV peaks in the 691-gated spectrum. These enhancements are caused by direct feeding of the 2326.0- and 2382.6-keV levels, respectively, by the 690.6- and 692.4-keV components of the triplet. The conversion coefficients of the 691.2-keV γ ray were determined from the K- and L-electron intensities, which required only a 6% correction for the other two weaker, $E1$, components of the triplet. The four γ-ray branches to states of known $J^\pi = 2^+$, 4^+, 5^+, and 6^+, with $M1$ multipolarity to the 5^+ and $E2$ to the 2^+, requires $J^\pi = 4^+$ for the 3094.5-keV level.

The γ-γ coincidence data in Fig. 5 provide strong evidence that a level at 3219.0 keV is depopulated by the 780.6-keV γ ray. All the prominent peaks in coincidence with this γ ray are associated with decay of the 7_1^+ level at 2438.4 keV. In addition, a weak 1030.6-keV γ ray appears in coincidence with the 631.0-keV $8_2^+ \rightarrow 8_1^+$ transition, and the 1746.0-keV γ-ray energy fits well for decay to the 6_1^+ state. We could not expect to detect this weak γ ray in coincidence with decay of the 6_1^+ level. The 3219.0-keV level must have positive parity because of the $M1$ component in the 780.6-keV γ ray. A spin of 6 would agree with all the decay data and with the shell-model prediction of the $\pi(f_{7/2}^2)_6$ state at about this energy, but we have no strong model-independent argument for rejecting a spin of 7.

The 2^+ state of the $f_{7/2}^2$ configuration is expected to lie at $\sim$2.9 MeV of excitation and to decay predominantly to the ground state (see Sec. IV). Therefore, it is not surprising that we find no evidence for this level in the coincidence data. However, there are three γ rays in this region, at 2771.6, 2795.5, and 2867.9 keV, whose excitation functions clearly show that they depopulate low-spin states. The extrapolation of the electron efficiency calibration out to these energies is somewhat risky, but the K-conversion coefficients thus obtained strongly suggest $E1$ multipolarity for the 2771.6- and 2795.5-keV γ rays and $E2$ or $M1$ for the 2867.9-keV. With an energy that is very close to the prediction of 2.9 MeV and a cross section about 20% of that for the 2290.1-keV 2^+ level, the 2867.9-keV γ ray is a good candidate for the $2^+ \rightarrow 0_1^+$ transition from the $f_{7/2}^2$ configuration.

TABLE II. Measured conversion-electron energies and the deduced transition energies for the 2614.6-keV transition in ^{208}Pb and the transition near 2608 keV assumed to occur in Po, Bi, or Pb.

		E_γ (keV)[a]		
shell	E_e (keV)[a]	Po	Bi	Pb
K	2526.66(3)			2614.67(3)
L_1	2598.78(11)			2614.64(11)
K	2515.45(8)	2608.56(8)	2605.98(8)	2603.46(8)
L_1	2591.98(79)	2608.88(79)	2608.33(79)	2607.83(79)

[a]Statistical errors in the least significant digits are given in parentheses.

C. The $\pi h_{9/2} i_{13/2}$ configuration

The previous experimental work[6] has identified possible candidates for nine of the ten states of this configuration. No evidence for the 3^- state has been reported, and definite spin-parity assignments have been made only for the states of 2849.1 and 3026.2 keV with $J^\pi = 11^-$ and 5^-, respectively. Groleau *et al.*[7] proposed levels for all but the $J^\pi = 3^-$ state on the basis of proton l-transfer data and spectroscopic factors. Our data are in good agreement with the previous work for the well-established states at 3026.4 keV ($J^\pi = 5^-$) and 2849.2 keV ($J^\pi = 11^-$).

The spectrum in Fig. 5 in coincidence with the 637.0-keV γ ray indicates that this transition populates the 3_1^- state at 2386.8 keV from a level at 3023.7 keV. Additional support for the 3023.7-keV level is provided by the energy fit of a second depopulating γ ray of 609.9 keV to the 2413.8-keV 3_1^+ state. The excitation function indicates a low spin, and the $M1$ multipolarity of the 637.0-keV γ ray restricts the spin-parity possibilities for the 3023.7-keV level to $(2,3,4)^-$. This may be the same level that Groleau *et al.* reported at 3028 keV and assigned $J^\pi=2^-$.

The spectra in Fig. 5 require γ-ray coincidence cascades of 1664.6-1181.4 and 459.0-1205.4-1181.4 keV, indicating a previously unobserved level at 2846.0 keV which is depopulated by the 1664.6- and 459.0-keV γ rays. The excitation functions indicate a low spin, and the multipolarities of $E1$ to the 2_1^+ state and $M1$ to the 3_1^- state restrict the spin-parity possibilities for the 2846.0-keV state to $J^\pi=(2,3)^-$.

A level at 3075.2 keV is supported by the observation of four γ-ray coincidence cascades. The 1648.4-245.3-1181.4 keV cascade (Fig. 5) provides clear evidence of the level, and the other three weaker depopulating γ rays are detected in the appropriate coincidence slices. Only the 1648.4-keV depopulating γ ray could be measured in the excitation-function runs; the data indicate a low spin for the depopulated level. Gamma branches to 4^+, 3^+, and 3^- states, and $E1$ multipolarity for the transition to the 4_1^+ state restrict the spin-parity possibilities for the 3075.2-keV state to $J^\pi=(3,4)^-$. The only previous evidence for this state is the observation of the 1648.4-keV γ ray in ^{210}At β decay[10] and a level at 3079 keV reported by Groleau *et al.*[7] and assigned $J^\pi=4^-$.

Coincidence gates on the 721.8- and 799.2-keV γ-ray peaks show that these transitions depopulate the level at 3125.1 keV. The conversion coefficients restrict the spin-parity of the 3125.1-keV state to $J^\pi=(5,6)^-$. Previously, the 722- and 799-keV γ rays were observed in the ^{210}At decay[10] and tentatively attributed to depopulation of a level at 3124.7 keV, and Groleau *et al.*[7] assigned $J^\pi=6^-$ to a level at 3125 keV populated by the (α,t) reaction.

Levels observed by Fant[8] in ^{208}Pb $(\alpha,2n\gamma)$ experiments and by Groleau *et al.*[7] in proton transfer have been proposed for the 7^-, 8^-, 9^-, and 10^- states, at 3016.6, 3137.8, 2999.5, and 3182.7 keV, respectively. However, none of the spins or parities were uniquely determined. Our γ-γ prompt and delayed coincidence data are in excellent agreement with the level placements. In addition, our measured conversion coefficients require negative parity for each of the states, and for the 3182.8-keV level they uniquely determine $J^\pi=10^-$.

D. The $\nu g_{9/2}p_{1/2}^{-1}$ configuration

The earlier reaction and β-decay measurements have identified a 5^- state at 2910 keV with the $\nu g_{9/2}p_{1/2}^{-1}$ configuration, based on its strong population by β decay of ^{210}At. Our coincidence and conversion-coefficient data agree with the placement of this level and with $J^\pi=5^-$.

Gamma rays of 1684.6 and 724.7 keV from a level at 3111.5 keV were observed in the β-decay measurements, but the weak population from ^{210}At decay was used to reject a $\nu(g_{9/2}p_{1/2}^{-1})_{4^-}$ assignment.[10] However, a close look at the angular-momentum coupling shows that β decay from the $(\pi h_{9/2}^3 \nu p_{1/2}^{-1})_{5^+}$ state in ^{210}At to the $\nu g_{9/2}p_{1/2}^{-1}$ configuration in ^{210}Po strongly favors the 5^- over the 4^- state. Our experiments populated this level much more strongly, and we were able to observe two additional depopulating γ rays supported by γ-γ coincidences. We place the 201.6-keV γ transition between the 3111.6- and 2910.9-keV levels on the basis of strong coincidences with the 1483.4- and 1436.7-keV γ rays that depopulate the 2910.0-keV level (Fig. 7). The 201.6 γ ray may be a doublet, with the other component depopulating the level at 3727.2 keV to the 3525.3-keV level as suggested by Jardine *et al.*[10] However, this branch is only barely, if at all, detectable in our coincidence data for the γ rays that depopulate the 3525.3-keV level.

The conversion coefficients for the γ rays that depopulate the 3111.6-keV level indicate an $E1$ transition to the 4_1^+ state, $M1$ (Jardine *et al.*) or $M1+E2$ (this work) to the 3_1^- state, and $M1$ to the 5_1^- state. These data require $J^\pi=4^-$ for the 3111.6-keV state. The fourth (728.4-keV) γ ray is consistent with this picture if we interpret the conversion coefficient $\alpha_K=0.020\pm0.010$ as arising from an $E1/M2$ rather than $M1/E2$ mixture.

E. States above 3220 keV

The level at 3428.6 keV was identified in the β-decay measurements of Jardine *et al.*,[10] who observed seven depopulating γ rays. We detected six of the γ rays and determined $E1$ multipolarity for the 1955.1-keV γ ray to the 6_1^+ state. This result, combined with the other multipolarities from our data and those of Jardine *et al.*, requires $J^\pi=5^-$ for the 3428.6-keV level.

The β-decay data showed a level at 3525.2 keV that is depopulated by four γ rays. Our coincidence data show a fifth γ ray, of 1122.0 keV, which also appears to be barely detectable in the published γ-ray spectrum of Jardine *et al.*[10] The conversion-coefficient measurements of Jardine *et al.* agree with $M1$ multipolarity for the 499.1- and 615.3-keV γ rays, requiring negative parity for the 3525.3-keV level. Our conversion coefficient for the 615.3-keV γ ray requires a substantial $E2$ mixture, but the negative parity of the 3525.3-keV state seems clearly established nevertheless. The spin is determined to be 6, based on the conversion coefficients shown in Table I, which require a dipole component in transitions to states with spins of 5, 6, and 7.

We find a new state at 3685.4 keV with $J^\pi=7^-$. The decay of this state to the 6_2^+, 8_2^+, and 8_1^+ levels is indicated by observation of the 1359.6-852.7, 1497.4-631.0 (Fig. 7), and 2128.1-245.3 (delay) keV γ-ray coincidence cascades. The fourth depopulating γ ray, of 2211.8 keV, is marginally detectable in delayed coincidence with the 245.3-keV $4_1^+\rightarrow2_1^+$ γ transition. The $E1$ multipolarities for γ rays to 6^+ and 8^+ states require $J^\pi=7^-$ for the 3685.4-keV state.

Jardine *et al.*[10] interpreted γ rays of 2272.7 and 2226.0 keV seen in β decay as depopulating a level at 3699.4

keV. The two γ rays that we see at 2272.9 and 2226.6 keV agree with this interpretation, and in addition the 2272.9-keV γ-ray peak appears weakly in coincidence with the $4_1^+ \rightarrow 2_1^+$ 245.3-keV transition. However, the intensity of our 2226.6-keV γ ray relative to the 2272.9 is larger than in Jardine's data, so we may have a contaminant peak at 2226.6 keV. Our data in Table I also show three other γ rays whose energies and excitation functions are in satisfactory agreement for depopulating the 3699.6-keV level. The conversion coefficients of the 2272.9- and (possibly contaminated) 2226.6-keV γ rays require negative parity and suggest a spin of 5 for the 3699.6-keV state.

In the ^{210}At decay there was tentative evidence for a level at 3711.2 keV, based on γ rays of 2284.5 and 2237.9 keV that would depopulate the level to the 4_1^+ and 6_1^+ states, respectively. Our γ rays of 2284.4, 2238.2, and 1307.3 keV agree with decay from such a level, at 3711.0 keV. In addition we have tentative evidence for a 2284.4-245.3 keV prompt coincidence cascade. The spin parity of the 3711.0-keV level is most likely 5^-, based on $E1$ multipolarity to the 6_1^+ state and γ-ray branches to the 4_1^+ and 5_1^+ states.

The levels at 3727.3 and 3779.9 keV were assigned from the ^{210}At decay studies. Our coincidence data, which show the 817.2- (1483.4, 1436.7)- and 1289.3-250.4-keV γ-ray cascades from the 3727.3-keV level and the 2353.0-245.3- and 870.0- (1483.4, 1436.7)-keV cascades from the 3779.9-keV level, solidify these assignments. Our conversion-coefficient measurements and those from ^{210}At decay show that both these states have negative parity, but the spins are not uniquely determined.

New levels at 3780.2 and 4025.8 keV are indicated by depopulating γ rays of 1592.2 and 1837.8 keV, respectively. Figure 7 shows that these γ rays are in prompt coincidence with the 631.0-keV 8_2^+ to 8_1^+ transition. They also appear in coincidence with the delayed 245.3- and 1181.4-keV γ-ray gates. For each of these levels we see a second possible depopulating γ ray that was too weak to be clearly detected in coincidence. (There is some evidence of the 1453.7-keV γ ray in delayed coincidence with the 245.3-keV γ ray.) The conversion coefficients in Table I would require $J^\pi = 7^-$ for the 3780.2-keV level, but we consider the placement of the 1453.7-keV γ ray too tentative to allow a unique spin determination. For the 4025.8-keV level the dipole component in the 1837.8-keV transition limits the possible spins to 7–9.

The remaining levels that we see have $J \gtrsim 10$ and were populated much more strongly in the 17-MeV runs. The γ-γ coincidence data shown in Fig. 7 indicate that the 962.6-keV γ ray depopulates a level at 4145.4 keV. This is supported by a second depopulating γ ray of 1146.5 keV that appears in the 1146.5-811.5-631.0-245.3(del) coincidence cascade. The coincidence data in Fig. 7 also indicate that a 178.8-keV transition populates this level from the well-known 4324.1-keV 11^- level. We cannot determine a unique spin for the 4145.4-keV state, but γ-ray feeding from the 11^- state and γ decay to the $(9)^-$ state combined with the conversion coefficients suggests that $J^\pi = (10)^-$ is the most likely choice. In previous work[6] Groleau *et al.* reported a level at 4139 keV with a suggested J^π of 6^+, and the (d,d') study showed a level at 4146 keV.

The levels at 4324.1, 4371.9, 4777.3, and 5057.6 keV with $J^\pi = 11^-$, 13^-, 14^-, and 16^-, respectively, have been well characterized by the $(\alpha,2n)$ yrast studies.[9,17] Our γ-γ coincidence data with 17-MeV tritons agree with these results. In addition, we have evidence for two new levels in this region, at 4502.8 and 4971.3 keV. The appearance of a 178.8-keV γ ray (Fig. 7) in strong prompt coincidence with the 1474.9-keV γ ray indicates that the 4502.8-keV level decays to the 4324.1-keV level. Additional γ-γ coincidence support for the 4502.8-keV level is provided by the 1653.4-1292.2(del)-245.3(del)-keV cascade. The 1653.4-keV γ ray appears convincingly in coincidence with the delayed 245.3-keV gate and marginally with the delayed 1292.2-keV gate. The third depopulating γ ray is placed only on the basis of a reasonable energy fit. There is also evidence that the 274.2-keV γ ray populates the 4502.8-keV level. The energy fit and excitation function (clearly indicating a high-spin state) of the 274.2-keV γ ray are reasonable and the 274.2-keV γ ray may appear very weakly in coincidence with the 178.8- and 1474.9-keV γ rays. The 4502.8-keV state most likely has $J^\pi = 12^-$, based on population from the 14^- state and decay with $M1$ multipolarity to the 11_1^- state.

The level at 4971.3 keV is based mainly on the observed depopulation by the 599.5-keV γ ray, which appears in coincidence with the delayed 1522.8-, 1474.9- (Fig. 7), and 1292.2-keV γ-ray gates. These gates also show the 405.5-keV γ ray from the 4777.3-keV level and a 557.1-keV γ ray which may come from an unidentified level in ^{210}Po. The 4971.3-keV state most likely has $J^\pi = 11^-$ or 12^-, assuming that it decays to states with $J^\pi = 10^-$ and 13^-.

F. Isomeric half-lives

There are six known states, namely the yrast levels with $J^\pi = 4^+$, 6^+, 8^+, 11^-, 13^-, and 16^+, that have measurable half-lives of greater than 1 ns. Recent mea-

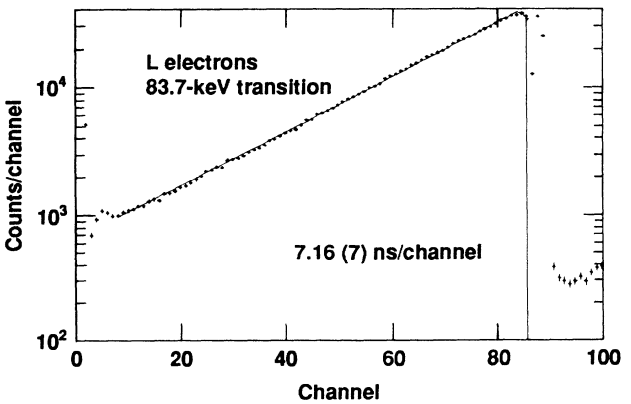

FIG. 8. Decay of L-conversion electrons from the 83.7-keV $8_1^+ \rightarrow 6_1^+$ transition. Data were fitted by an exponential plus a constant background.

TABLE III. Measured lifetimes of the four highest isomeric states in ^{210}Po.

Energy (keV)	J^π	Half-life (ns) This work[a]	Ref. 6	Recent work
5057.6	16^+		6700 syst.	262(3)[a,b] 262(6)[c]
4371.9	13^-	56.1(14)	93(6)	51(2)[d] 48.7(5)[a,b]
2849.2	11^-	19.6(4)	20.4(10)	20.4[b]
1557.0	8^+	101.0(12)	96.0(14)	

[a]The error in the least significant digits (in parentheses) is the statistical fitting error combined with a 1% calibration error.
[b]Reference 18.
[c]Reference 9.
[d]Reference 17.

surements[9,17] on the 16^+ and 13^- levels gave half-lives that differ substantially from the earlier values.[6] Our conversion-electron data yielded accurate measurements of the 13^-, 11^-, and 8^+ half-lives. Figure 8 shows the decay of L-shell electrons from the 83.6-keV $8^+ \rightarrow 6^+$ transition; these data were combined with M-shell data of comparable quality to obtain a half-life of 101.0±1.2 ns for the 8_1^+ state. In Table III we summarize the lifetime measurements from the 16^+, 13^-, 11^-, and 8^+ isomers, including our results from a recent study[18] of the electric quadrupole moments in ^{210}Po.

IV. DISCUSSION

These experiments, combined with previously published data,[6–10] firmly identify all the levels of the $\pi h_{9/2} f_{7/2}$ configuration, and they establish the negative parity and probable spins of ten levels that most likely are the complete set of levels associated with the $\pi h_{9/2} i_{13/2}$ configuration. In addition, we have identified strong candidates for the 0^+, 4^+, and 6^+ levels, and possibly the 2^+ level, of the $\pi f_{7/2}^2$ configuration. In the following discussion we will compare the data in Table I for these levels with calculated energies and γ-ray branching ratios based on the above configurations. The effective single-particle matrix elements for calculating the $M1$ and $E2$ γ-transition rates were obtained from Refs. 18 and 19 and are listed in Table IV. These are all experimentally determined except for the $\langle f_{7/2} \| \vartheta \| f_{7/2} \rangle$ elements, which are obtained from reliable calculations and systematics in the ^{208}Pb region.

We will calculate γ-ray branching ratios for three different sets of wave functions: pure configurations, the Kuo-Herling[20] wave functions limited to the $h_{9/2}^2$, $h_{9/2} f_{7/2}$, and $f_{7/2}^2$ configurations, and an optimized mixing of the $h_{9/2}^2$ and $h_{9/2} f_{7/2}$ configurations. Our use of effective matrix elements is appropriate for calculations with pure configurations and with mixed wave functions restricted to the $h_{9/2}$ and $f_{7/2}$ orbitals. On the other hand, the Kuo-Herling wave functions are calculated for a large configuration space and should require different transition matrix elements. We will address this point later in our discussion of transitions from the $h_{9/2} f_{7/2}$ levels.

TABLE IV. Transition-rate matrix elements from Refs. 18 and 19.

	$M1$ (μ_N)	$E2$ (e fm)^2
$\langle h_{9/2} \| \vartheta \| h_{9/2} \rangle$	6.97	−59.6
$\langle f_{7/2} \| \vartheta \| h_{9/2} \rangle$	0.18	−15.5
$\langle f_{7/2} \| \vartheta \| f_{7/2} \rangle$	8.41	−53.5

A. Energies of two-particle states

In Fig. 9 we show the levels of the four lowest two-proton configurations in ^{210}Po as established in this experiment, together with the unperturbed single-particle

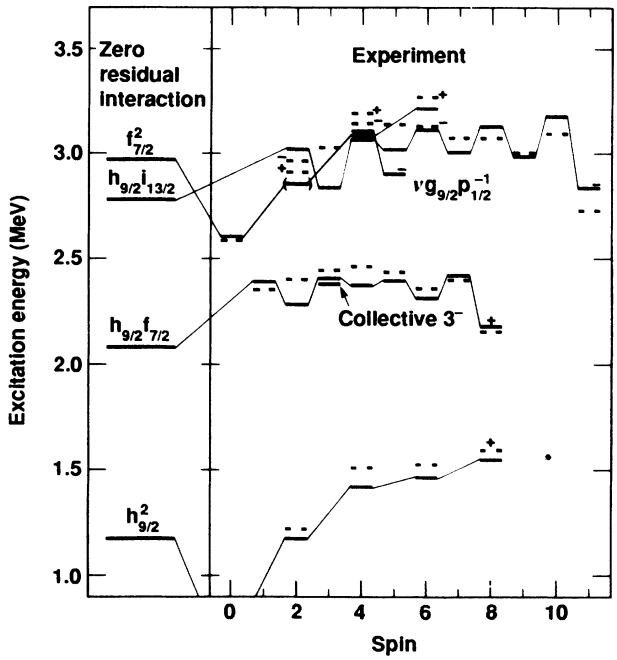

FIG. 9. Measured level energies of the four lowest two-proton configurations in ^{210}Po compared with the single-particle energies (left) and with the calculated energies (dashed lines) from Kuo-Herling. The Kuo-Herling ground state is at −400 keV in this plot. The measured energies of the collective 3^- and $\nu g_{9/2} p_{1/2}^{-1}$ core states are also shown.

energies for comparison. The two 0^+ states are lowered appreciably with respect to the single-particle predictions. Otherwise, the residual interaction is repulsive and weak ($\sim$200 keV) and exhibits little dependence on spin. Configuration mixing is not very important except for the 4^- and 5^- levels, and to a lesser extent the 3^-, for which core states of the same spin and parity (also shown in Fig. 9) lie nearby in energy. Therefore the experimental energies give directly the matrix elements of the residual interaction. Figure 9 also shows the calculated energies from the work of Kuo and Herling,[20] with the ground state placed at -400 keV. Except for this discrepancy in the ground state, the calculated energies agree typically within 100 keV with the experimental energies.

B. Decay from the $h_{9/2}f_{7/2}$ configuration

Gamma decay of the $h_{9/2}f_{7/2}$ levels is summarized in Table V. All these levels decay to the $h^2_{9/2}$ levels, and at least half of the $M1$ and $E2$ transitions that are allowed by the spins are strong enough to be detected in our experiments. In addition the odd-spin levels, which all lie above the even spins, decay by intramultiplet low-energy (20–250 keV) $M1$ transitions to the even-spin states.

For calculating the theoretical transition rates with the matrix elements from Table IV, we first assumed pure configurations. This should be particularly well justified for the odd spins, because there are no nearby states with which to mix. The calculated γ-ray branching ratios are shown in the first column of calculations in Table V. In the next column we show the results obtained by using the Kuo-Herling wave functions, arbitrarily limited to the $h^2_{9/2}$, $h_{9/2}f_{7/2}$, and $f^2_{7/2}$ configurations. Clearly, the γ-decay rates will be highly sensitive to admixtures in the wave functions, because transitions between the $h_{9/2}f_{7/2}$ and $h^2_{9/2}$ main components of the wave functions proceed only through the weak matrix elements $\langle f_{7/2}\|M1$ or $E2\|h_{9/2}\rangle$. This is l forbidden for $M1$ and involves a spin flip for $E2$, whereas for mixed configurations the much stronger diagonal elements contribute.

To illustrate the extreme sensitivity of the $M1$ transition rates to admixtures in the wave functions we consider the decay of the pure $(h_{9/2}f_{7/2})_{7^+}$ state to the 6^+_1 and 8^+_1 levels. For mixing amplitudes of only a few percent or less, the 6^+_1 and 8^+_1 wave functions can be written as

$$|6^+\rangle = h^2_{9/2} + a(h_{9/2}f_{7/2}) + bf^2_{7/2} ,$$
$$|8^+\rangle = h^2_{9/2} + c(h_{9/2}f_{7/2}) .$$

This gives the $M1$ matrix elements (in μ_N)

$$\langle 6^+\|M1\|7^+\rangle = 0.047 + 2.27a - 0.29b ,$$
$$\langle 8^+\|M1\|7^+\rangle = 0.31 - 1.77c .$$

Kuo-Herling (approximation 3, Coulomb) give $a=-0.04$, $b=0.03$, and $c=-0.07$, which gives a reversal of the sign of $\langle 6^+\|M1\|7^+\rangle$ but only a slight increase in magnitude, so there is little change in $B(M1)$. Therefore, a comparison between the results for the pure and the mixed Kuo-Herling wave functions can be misleading. However, we see that in this case the transition element between the main components is so weak that the admixtures become dominant. Big, but less drastic, changes also occur for $E2$ transition rates.

These results then suggest a highly sensitive approach for determining the admixtures to the wave functions, by using the measured γ-ray branching ratios. We have done this, restricting the wave functions to $h^2_{9/2}$ and $h_{9/2}f_{7/2}$ only and requiring orthogonality. Thus, only the even-spin states are mixed. First the 8^+ wave functions were adjusted to reproduce the observed $M1/E2$ intensity ratio in the $8^+_2 \rightarrow 8^+_1$ transition. Then the 6^+ wave functions were adjusted to optimize the agreement between calculated and observed branching ratios from the 7^+ state. Finally, the admixtures to the 4^+ and 2^+ wave functions were determined by trial in similar fashion, with the constraint of keeping admixtures as small as possible. The third column of calculated branching ratios in Table V shows the results obtained from this optimization procedure.

The three sets of calculations in Table V show that pure wave functions reproduce the many measured branching ratios quite well. The optimized mixed wave functions, in which the admixture amplitudes are $\leq 4\%$, improve the agreement significantly; only four $E2$ transitions disagree appreciably with the measurements. The wave functions from Kuo and Herling which have larger, but still small, configuration mixing yield no improvement over pure states. In fact, the comparisons in Table V suggest that Kuo-Herling give too much mixing. The calculated results are not very sensitive to the value of the $\langle f_{7/2}\|M1\|f_{7/2}\rangle$ matrix element, which has not been measured directly. The uncertainty is $\sim 5\%$, and a change of this magnitude changes the $B(M1)$'s of transitions within the $h_{9/2}f_{7/2}$ multiplet by about 20%. This comes about because typically the $h_{9/2} \rightarrow h_{9/2}$ transition cancels 50% of the $f_{7/2} \rightarrow f_{7/2}$ (they have opposite signs) in the transition element between the two-particle states. All other transition rates remain practically unchanged.

Our calculated transition rates could possibly be affected by certain orbitals that we have neglected. The next higher orbitals of negative parity that might be important are the $f_{5/2}$ and $p_{3/2}$, which lie at about 2 and 3 MeV, respectively, above the $f_{7/2}$ energy. For a qualitative discussion of their influence we will classify the transitions as "allowed" or as "hindered" by various degrees. Thus the $M1$ transitions within the $h_{9/2}f_{7/2}$ multiplet, which proceed with strong matrix elements between the dominant configurations of the states, are allowed. Transitions that involve either a weak matrix element between the dominant configurations, or a strong matrix element between the dominant configuration of one state and a small component in the other state, have one degree of hindrance. Transitions from $h_{9/2}f_{7/2}$ to $h^2_{9/2}$ are hindered in this sense. Admixtures of the higher orbitals will be regarded as important only if they lead to transitions of the same rank as those found in the space restricted to the $h_{9/2}$ and $f_{7/2}$ orbitals. Thus, transitions within the $h_{9/2}f_{7/2}$ multiplet involve only the allowed

TABLE V. Measured γ-ray branching intensities from states of the $\pi h_{9/2}f_{7/2}$ configuration in ^{210}Po compared with calculated intensities based on pure configurations, Kuo-Herling wave functions, and an optimized mixing.

$\pi h_{9/2}f_{7/2}$		Final state				Branching intensity (%)			
E_x				E_γ			Calculation[a]		
(keV)	J_i^π	Config.	J_f^π	(keV)	Mult.	Expt.	Pure	K-H[b]	Mixed[c]
2398.8	1^+	$h_{9/2}^2$	0^+	2393	$M1$	73(5)	76	27	76
			2^+	1212	$M1$	27(5)	9	31	9
					$E2$		13	38	13
		$h_{9/2}f_{7/2}$	2^+	103	$M1$		2	3	2
Total γ-decay constant (10^{12} s^{-1})							0.69	0.32	0.69
2290.1	2^+	$h_{9/2}^2$	0^+	2290	$E2$	90(2)	87	85	88
			2^+	1108	$M1$	7(2)	11	14	11
					$E2$	3(2)	0	0	0
			4^+	863	$E2$		2	1	1
Total γ-decay constant (10^{12} s^{-1})							0.84	1.3	0.84
2413.8	3^+	$h_{9/2}^2$	2^+	1232	$M1$	34(7)	21	2	27
					$E2$	46(7)	31	27	40
			4^+	987	$M1$	13(2)	35	60	18
					$E2$		3	4	4
		$h_{9/2}f_{7/2}$	2^+	123	$M1$	7(2)	9	6	11
			4^+	31	$M1$		0.2	0.1	0.2
Total γ-decay constant (10^{12} s^{-1})							0.17	0.21	0.13
2382.6	4^+	$h_{9/2}^2$	2^+	1201	$E2$	6(1)	18	33	10
			4^+	955	$M1$	73(12)	50	40	62
					$E2$	16(12)	10	7	10
			6^+	909	$E2$	5.9(5)	22	20	19
Total γ-decay constant (10^{12} s^{-1})							0.097	0.096	0.11
2403.3	5^+	$h_{9/2}^2$	4^+	976	$M1$	35(7)	8	1	37
					$E2$	13(7)	16	10	19
			6^+	929	$M1$	32(4)	72	87	39
					$E2$	16(4)	1	0	1
		$h_{9/2}f_{7/2}$	4^+	20	$M1$	0.07(4)	0.06	0.04	0.08
			6^+	77	$M1$	3.2(9)	3.2	2.1	4.2
Total γ-decay constant (10^{-12} s^{-1})							0.096	0.14	0.075
2326.0	6^+	$h_{9/2}^2$	4^+	899	$E2$	1.8(3)	3.2	6	1.3
			6^+	852	$M1$	70(10)	55	51	73
					$E2$	25(10)	26	25	16
			8^+	769	$E2$	3.5(3)	16	18	10
Total γ-decay constant (10^{12} s^{-1})							0.043	0.037	0.078
2438.4	7^+	$h_{9/2}^2$	6^+	965	$M1$	14(3)	2	1	10
					$E2$	14(3)	5	3	5
			8^+	881	$M1$	30(5)	54	68	47
					$E2$	10(5)	9	7	9
		$h_{9/2}f_{7/2}$	6^+	112	$M1$	3.0(5)	4.0	2.9	3.9
			8^+	250	$M1$	30(3)	27	19	26
Total γ-decay constant (10^{12} s^{-21})							0.14	0.20	0.15
2188.0	8^+	$h_{9/2}^2$	6^+	714	$E2$	≈ 0	1	3	1
			8^+	630	$M1$	79(3)	66	82	76
					$E2$	21(3)	33	16	23
Total γ-decay constant (10^{12} s^{-1})							0.0054	0.0075	0.0083

[a]Calculated with matrix elements from Table IV.

[b]Reference 20.

[c]Optimized mixing as discussed in Sec. IV. The amplitudes of the $h_{9/2}f_{7/2}$ admixtures to the lower $h_{9/2}^2$ states are: 0.00 (2^+), 0.03 (4^+), 0.04 (6^+), and 0.01 (8^+). The admixtures of $h_{9/2}^2$ to the upper states have the same amplitudes but opposite signs.

$M1$ transitions between the dominant components. On the other hand, for the hindered transitions from $h_{9/2}f_{7/2}$ to $h^2_{9/2}$ we have to consider the $\langle h_{9/2}f_{5/2}\|E2\|h^2_{9/2}\rangle$, $\langle h_{9/2}f_{7/2}\|M1\|h_{9/2}f_{5/2}\rangle$, and $\langle h_{9/2}f_{7/2}\|E2\|h_{9/2}p_{3/2}\rangle$ matrix elements. The first of these is the most important and might well explain the discrepancies mentioned above in the $E2$ rates. Since no calculations were performed with the full Kuo-Herling wave functions, it is not clear how big the changes would be. An attempt to fit these additional components would involve many parameters, and in addition the matrix elements are not well known.

TABLE VI. Gamma-ray branching intensities from the states of the $\pi f^2_{7/2}$ configuration in ^{210}Po compared with calculated intensities based on pure configurations and on the Kuo-Herling wave functions.

$\pi f^2_{7/2}$		Final state				Branching intensity (%)		
							Calculation[a]	
E_x (keV)	J^π_i	Config.	J^π_f	E_γ (keV)	Mult.	Expt.	Pure	K-H[b]
2608.6	0^+	$h^2_{9/2}$	0^+		$E0$	yes		
		$h^2_{9/2}$	2^+	1427	$E2$	$>\sim 50$	0	100
		$h_{9/2}f_{7/2}$	1^+	214	$M1$	$<\sim 50$	85	0
		$h_{9/2}f_{7/2}$	2^+	318	$E2$	~ 0	15	0
Total γ-decay constant (10^{12} s^{-1})							0.0017	1.5
~ 2900	2^+	$h^2_{9/2}$	0^+		$E2$			91
		$h^2_{9/2}$	2^+		$M1$			0.9
		$h^2_{9/2}$	2^+		$E2$			0.6
		$h^2_{9/2}$	4^+		$E2$			3.4
		$h_{9/2}f_{7/2}$	2^+		$M1$		45	1.5
		$h_{9/2}f_{7/2}$	2^+		$E2$		6	0
		$h_{9/2}f_{7/2}$	4^+		$E2$		5	0
		$h_{9/2}f_{7/2}$	1^+		$M1$		3	1.9
		$h_{9/2}f_{7/2}$	1^+		$E2$		2	0
		$h_{9/2}f_{7/2}$	3^+		$M1$		36	1.1
		$f^2_{7/2}$	0^+		$E2$		3	0
Total γ-decay constant (10^{12} s^{-1})							0.027	4.8
3094.5	4^+	$h^2_{9/2}$	2^+	1913	$E2$	8(2)	0	8.3
		$h^2_{9/2}$	4^+	1667	$M1$	7(3)	0	50
					$E2$		0	4.3
		$h^2_{9/2}$	6^+	1621	$E2$		0	10
		$h_{9/2}f_{7/2}$	2^+	804	$E2$		1	1.0
		$h_{9/2}f_{7/2}$	4^+	711	$M1$		23	7.2
					$E2$		7	1.7
		$h_{9/2}f_{7/2}$	6^+	768	$E2$	9(3)	13	3.3
		$h_{9/2}f_{7/2}$	3^+	680	$M1$		3	13
					$E2$		3	0.4
		$h_{9/2}f_{7/2}$	5^+	691	$M1$	52(20)	49	0.2
					$E2$	24(20)	1	0.4
Total γ-decay constant (10^{12} s^{-1})							0.064	0.28
3219.0	6^+	$h^2_{9/2}$	4^+	1792	$E2$		0	0.1
		$h^2_{9/2}$	6^+	1745	$M1$	2(10)	0	56
					$E2$	14(10)	0	4.7
		$h^2_{9/2}$	8^+	1662	$E2$		0	4.8
		$h_{9/2}f_{7/2}$	4^+	836	$E2$		0.2	0
		$h_{9/2}f_{7/2}$	6^+	893	$M1$		15	4.6
					$E2$		12	5.2
		$h_{9/2}f_{7/2}$	8^+	1030	$E2$	6(3)	14	6.6
		$h_{9/2}f_{7/2}$	5^+	815	$M1$		1	8.8
					$E2$		2	0.7
		$h_{9/2}f_{7/2}$	7^+	780	$M1$	58(5)	49	5.8
					$E2$	20(5)	7	2.8
Total γ-decay constant (10^{12} s^{-1})							0.11	0.29

[a]Calculated with matrix elements from Table IV.
[b]Reference 20.

C. Decay from the $f_{7/2}^2$ configuration

The experimental and calculated γ-decay branching ratios from the $f_{7/2}^2$ levels are compared in Table VI. As for the $h_{9/2}f_{7/2}$ levels, we used the standard transition matrix elements in Table IV to calculate the transition rates both for pure and for mixed configurations. Again, all the important transition elements have been obtained from direct measurements. The diagonal $M1$ and $E2$ matrix elements for the $f_{7/2}$ orbital, which have not been directly measured, enter only in connection with small amplitudes of the wave functions. For the mixed wave functions we again considered only the $h_{9/2}^2$, $h_{9/2}f_{7/2}$, and $f_{7/2}^2$ configurations and used the Kuo-Herling amplitudes. There is obviously some configuration mixing, because we observe transitions to the $h_{9/2}^2$ states. For decay from the 2^+ state, in particular, the Kuo-Herling results suggest that the only detectable transition might be the $2^+ \rightarrow 0_1^+$ ground-state transition. However, our approach with the Kuo-Herling amplitudes gives in general too much branching to the $h_{9/2}^2$ configuration, indicating again, as we found for decay of the $h_{9/2}f_{7/2}$ states, that Kuo and Herling give too much mixing. The pure configurations reproduce the experimental results rather well for decay of the 4^+ and 6^+ levels to the $h_{9/2}f_{7/2}$ levels.

D. Decay from the $h_{9/2}i_{13/2}$ states

The $(h_{9/2}i_{13/2})_{10^-}$ state at 3182.8 keV lies high enough in energy to decay in part by intramultiplet $M1$ transitions to the 11^- and 9^- states. These $M1$ transition rates can be calculated from the known magnetic moments of the $h_{9/2}$ and $i_{13/2}$ protons. The experimental branching ratio from Table I is

$$\frac{I_{183}(10^- \rightarrow 9^-)}{I_{333}(10^- \rightarrow 11^-)} = 0.20 \pm 0.03 ,$$

which agrees reasonably well with the calculated value of 0.29. In addition there is an 11% $M2$ γ-ray branch to the $(h_{9/2}^2)_{8^+}$ level. The partial half-life of this $M2$ transition should be very similar to that of the $i_{13/2} \rightarrow h_{9/2}$ transition in ^{209}Bi, which is 0.30 ± 0.15 ns. This is about 1 order of magnitude greater than our calculated partial half-life of 0.01 ns for the $M1$ transitions, in reasonable agreement with the observed $M2/M1$ intensity ratio of 0.12.

The lower-spin states of the $h_{9/2}i_{13/2}$ configuration can decay by $E1$ transitions. Usually, $E1$ decays to the $h_{9/2}f_{7/2}$ configuration are favored over those to the $h_{9/2}^2$. This may reflect the well-known stronger mixing of $i_{13/2}$ with $(f_{7/2} \otimes \text{col.}3^-)$ than with $(h_{9/2} \otimes 3^-)$, which removes one degree of forbiddeness of the $E1$ transitions. A few percent of $M2$ admixture is found in the transitions from the 8^- and 9^- states to the $(h_{9/2}^2)_{8^+}$. As we mentioned for the 10^- level, the decay constants for these $M2$ transitions should be $\sim 10^9$/s. Therefore, the observed $E1/M2$ intensity ratios indicate $E1$ transition probabilities of $\sim 10^{11}$/s, to be compared with $\sim 10^{16}$/s for the single-particle estimates.

The half-life and γ-ray branching of the 11^- state gives

$$B(E3, 11^- \rightarrow 8_1^+) = 9600 \pm 400 \ e^2\,\text{fm}^6$$

and

$$B(E3, 11^- \rightarrow 8_2^+) = 4900 \pm 3000 \ e^2\,\text{fm}^6 .$$

These results change slightly the values adopted by Bergström and Fant[21] in their review of the systematics of $B(E3)$ values in this region.

E. Conclusions

The level scheme of the four lowest-lying two-proton configurations in ^{210}Po relative to the ^{208}Pb core is now virtually complete, with probably only one exception [the $(f_{7/2}^2)_{2^+}$ state]. This level scheme provides a set of the residual interactions for shell-model calculations in this region of nuclei. The gamma transition rates are extremely sensitive to configuration mixing. The agreement between the measured and calculated γ-ray branching ratios proves the validity of the shell model with practically pure configurations.

ACKNOWLEDGMENTS

We highly appreciate many useful hints and discussions with Jan Blomqvist, Stockholm. We also acknowledge with pleasure the technical support provided by Allen Friensehner during these experiments. This work was performed by the Lawrence Livermore National Laboratory supported in part by the United States Department of Energy under Contract No. W-7405-Eng-48, and in part by Innovative Science and Technology-Strategic Defense Initiative Office, directed by the Naval Research Laboratory.

---

*On leave from Hahn-Meitner Institut, Berlin, Germany.

[1] K. H. Maier, T. W. Nail, R. K. Sheline, W. Stöffl, J. A. Becker, J. B. Carlson, R. G. Lanier, L. G. Mann, G. L. Struble, J. A. Cizewski, and B. H. Erkkila, Phys. Rev. C **27**, 1431 (1983).

[2] D. J. Decman, J. A. Becker, J. B. Carlson, R. G. Lanier, L. G. Mann, G. L. Struble, K. H. Maier, W. Stöffl, and R. K. Sheline, Phys. Rev. C **28**, 1060 (1983).

[3] J. A. Becker, R. G. Lanier, L. G. Mann, G. L. Struble, K. H. Maier, L. E. Ussery, W. Stöffl, T. W. Nail, R. K. Sheline, J. A. Cizewski, B. H. Erkkila, and J. Blomqvist, Phys. Rev. C **29**, 1268 (1984).

[4] K. H. Maier, M. Menningen, L. E. Ussery, T. W. Nail, R. K. Sheline, J. A. Becker, D. J. Decman, R. G. Lanier, L. G. Mann, W. Stöffl, and G. L. Struble, Phys. Rev. C **30**, 1702 (1984).

[5] K. H. Maier, in *International Conference on Nuclear Structure Through Static and Dynamic Moments*, edited by H. H. Bolotin (Conference Proceedings Press, Melbourne, 1987), Vol. 2.

[6]B. Harmatz, Nucl. Data Sheets **34**, 735 (1981).
[7]R. Groleau. W. A. Lanford, and R. Kouzes, Phys. Rev. C **22**, 440 (1980).
[8]B. Fant, Phys. Scr. **4**, 175 (1971).
[9]A. Källberg, Phys. Scr. **31**, 125 (1985), and references cited therein.
[10]L. J. Jardine, S. G. Prussin, and J. A. Hollander, Nucl. Phys. **A190**, 261 (1972).
[11]W. Stöffl and E. A. Henry, Nucl. Instrum. Methods **227**, 77 (1984).
[12]B. Rubio, P. Kleinheinz, A. Ercan, R. Julin, L. G. Mann, W. Stöffl, E. A. Henry, V. Dave, and J. Blomqvist, Proceedings of the XX Winter School Zakopane, 1985, Institute of Nuclear Physics, Kramow, Report No. 1302/PS, 1985, p. 369.
[13]J. W. Sunier, R. V. Poore, and D. E. McMillan, IEEE Trans. Nucl. Sci. **NS-26**, 4485 (1979).
[14]W. Stöffl, Technical University, Munich, Germany, 1980, Computer Code, FITEK (private communication).
[15]R. W. Hoff and J. M. Hollander, Phys. Rev. **109**, 447 (1958).
[16]J. K. Kantele, in *Heavy Ions and Nuclear Structure,* edited by B. Sikora and Z. Wilhelmi (Harwood Academic, New York, 1984), Vol. 5, p. 391.
[17]I. Bergström, J. Blomqvist, P. Carle, B. Fant, A. Källberg, L. O. Norlin, K.-G. Rensfelt, and U. Rosengard, Phys. Scr. **31**, 333 (1985).
[18]K. H. Maier, A. Berger, D. J. Decman, J. A. Becker, R. J. Estep, E. A. Henry, L. G. Mann, R. A. Meyer, N. Roy, and W. Stöffl, Lawrence Livermore National Laboratory Report UCAR 10062/86, 1986, pp. 4–72; K. H. Maier *et al.* (unpublished).
[19]D. J. Donahue, O. Häusser, R. L. Hershberger, R. Lutter, and F. Riess, Phys. Rev. C **12**, 1547 (1975).
[20]T. T. S. Kuo and G. H. Herling, U.S. Naval Research Laboratory Report No. 2258, 1971 (unpublished); T. T. S. Kuo, Nucl. Phys. **A122**, 325 (1968).
[21]I. Bergström and B. Fant, Phys. Scr. **31**, 26 (1985).